

Intracerebral Hematoma Extends via Perivascular Spaces and Perineurium

Jia Yin,¹ Tian-Ming Lü,¹ Guang Qiu,¹ Rui-Yu Huang,¹ Min Fang,¹
Yuan-Yuan Wang,¹ Duan Xiao¹ and Xiao-Jia Liu¹

¹Department of Neurology, Nanfang Hospital, Southern Medical University, Guangzhou, P.R. China

Intracerebral hemorrhage (ICH) is a devastating disorder associated with high morbidity and mortality. ICH results in the formation of hematoma that affects not only the primary site of injury but also the remote regions. In fact, hematoma can extend via perivascular spaces (also called Virchow–Robin spaces, VRS) and perineurium in an animal model of ICH. In the present study, we used magnetic resonance imaging (MRI) with susceptibility-weighted imaging (SWI) to investigate the characteristics of the perivascular and perineural extensions of hematomas in patients with ICH. A total of 20 ICH patients without secondary subarachnoid and secondary intraventricular hemorrhages were recruited. Brain MRI scans, including SWI, T1, and T2-weighted images, were performed between 17 h to 7 days after the onset of ICH. MRI with SWI revealed that paramagnetic substances spread along the VRS or the perineurium. Such distribution could cause the formation of cerebral microbleeds (CMBs). However, the distribution of remote hemorrhagic lesions varied, depending on the size and location of the original hematoma. The unenhanced CT scans of the 20 patients did not show any hyperdensity around the blood vessels and nerve tracts outside the hematoma. These results indicate the perivascular and perineural extensions of hematomas in patients with ICH, which is formed by the leakage of the original hematoma via the VRS or perineurium. We also provide a new explanation for the series of pathological processes involved in ICH, including the remote effects of hematoma and the formation of CMBs in patients with ICH.

Keywords: computed tomography; intracerebral hemorrhage; magnetic resonance imaging; perineurium; Virchow–Robin space

Tohoku J. Exp. Med., 2013 July, **230** (3), 133-139. © 2013 Tohoku University Medical Press

Introduction

Intracerebral hemorrhage (ICH) is a devastating disorder associated with high morbidity and mortality. The impact of an ICH is not only restricted to the primary site of injury, but also identified in the remote regions (Mun-Bryce et al. 2004; Menon et al. 2012). But the pathophysiological mechanisms of the remote effects of hematoma remain unknown, despite the important implications for both prognosis and treatment in the clinical practice of ICH. Our recent animal studies indicated that the hematomas can extend via perivascular spaces (also called Virchow–Robin spaces, VRS) and perineurium after experimental ICH, called perivascular and perineural extensions of hematomas (Lü et al. 2005, 2007; He et al. 2012). The results revealed that numerous ring hemorrhage lesions extended from the hematomas into perihematomal tissues, formed by the overflow of blood from the hematomas along VRS and perineurium (Lü et al. 2005, 2007). The distribution of formed and soluble blood elements varied during perivascular and peri-

neural extensions for different patterns of granular and amorphous materials. Both formed and soluble blood elements were drained into bilateral deep cervical lymph nodes. Furthermore, lymphostasis was observed in the brain tissues around the hematoma (He et al. 2012). The perivascular and perineural extensions of hematomas can provide the mechanism of the series of pathological processes involved in ICH such as the remote effects of hematoma and lymphostasis, which has emerged as a new focus in ICH research.

To date, no clinical study exists on the perivascular and perineural extensions of hematomas after ICH. Thus, we collected data of remote hemorrhagic lesions in acute ICH patients by using susceptibility-weighted imaging (SWI), which has emerged as a new technique for exploiting the magnetic differences between tissues to obtain excellent contrasts between tissues with susceptibilities (Haacke et al. 2004). We also studied the relationship between the original hematoma and remote hemorrhagic lesions to investigate the characteristics of the perivascular

Received February 26, 2013; revised and accepted May 31, 2013. Published online June 28, 2013; doi: 10.1620/tjem.230.133.

Correspondence: Tian-Ming Lü, Ph.D., Department of Neurology, Nanfang Hospital, Southern Medical University, No.1838 Guangzhou Ave, Guangzhou 510515, P.R. China.
e-mail: tianminglv@yeah.net

and perineural extensions of hematomas in human ICH.

Subjects and Methods

Convenience samples were chosen for this study from Feb 2008 to Sep 2011 at Nanfang Hospital. Patients with ICH in stable conditions without secondary subarachnoid and secondary intraventricular hemorrhages were arranged as candidates. A total of 20 patients were recruited in our study. Diagnoses were based on the clinical and neuroimaging evaluations of neurologists and neuroradiologists. Clinical data were collected by two stroke neurologists. All patients received neurological examinations and received noncontrast head computed tomography (CT) scans immediately after admission in our center. Magnetic resonance imaging (MRI) scans, including SWI, T1, and T2-weighted images (WI), were performed on the second day of admission. Considering the unstable condition of ICH patients, SWI data were collected by using quick echo-planar imaging (EPI). The interval between the onset of symptoms and the MRI scans was from 17 h to 7 days. Theoretically, blood from hematoma clotted and deoxygenated but not lysed at this time period. All pieces of equipment used in this study were approved by the State Food and Drug Administration. This study was conducted in accordance with the declaration of Helsinki, and with approval from the Ethics Committee of Nanfang Hospital. Written informed consent was obtained from all participants.

Data Acquisition

Noncontrast CT scanning was performed with a CT scanner (step-and-shoot mode; 140 kV; 111 mA; slice thickness, 10 mm).

MRI scanning was performed with a 3.0 T scanner. Magnetic resonance sequences included axial T1-WI, T2-WI, and SWI. The pulse sequences and typical parameters were as follows: (1) EPI-SWI gradient echo: repetition time (TR), 35 ms; echo time (TE), 25 ms;

flip angle, 60°; 20 slices; slice thickness, 3 mm; matrix size, 96 × 128; FOV, 240; acquisition time, 2 s; (2) T1-WI: TR, 2600 ms; TE, 23; flip angle, 90°; 20 slices; slice thickness, 5 mm; matrix size, 128 × 256; FOV, 240; acquisition time, 46 s; (3) turbo spin-echo T2/proton density (T2-WI): TR, 5100 ms; TE, 137/90 ms; flip angle, 180°; 20 slices; slice thickness, 5 mm; matrix size, 128 × 256; FOV, 240 mm; acquisition time, 1 min and 42 s. The original SWI images consisted of amplitude images and phase images, and the post-processing was performed at the workstation. Source phase images were processed through a low-pass filter to obtain corrected phase images. The obtained phase images subsequently underwent a series of post-processing such as phase mask, negative phase weighting, phase image and amplitude image multiplication, and minimal intensity projection to obtain SWI reconstructed images.

Subjects

The characteristics of the 20 patients are shown in Table 1. A total of 13 patients had putamen hematoma, 2 patients had thalamus hematoma, 2 patients had hematoma in the right parietal lobe, and 3 patients had multifocal supratentorial hematomas.

Results

Clinical Data

The MRI with SWI revealed remote hemorrhagic lesions, which was displayed as signal losses around the blood vessels or white matter outside the original hematoma (overall 100%, perivascular 80%, and white matter 40%). Most of them, measuring < 5 mm, belonged in cerebral microbleeds (CMBs). Twenty-five remote hemorrhagic lesions were observed at an average of 1.25/patient. The distribution of remote hemorrhagic lesions varied among

Table 1. Patient Characteristics and Signal Loss Distribution.

Patient No.	Sex / Age, y	Perivascular Foci	Perineural Foci	No. of Foci	Original Hematoma
1	M/69	L-MCA	No	1	L-putamen
2	F/56	L-sylvian cistern	L-basal ganglia	2	L-putamen
3	M/53	R-PCA	No	1	R-putamen
4	M/75	R-cortical segment	Bilateral supratentorial	1	Multifocal
5	M/34	R-internal cerebral veins	No	1	R-parietal lobe
6	F/62	No	R- midbrain	2	R-putamen
7	M/36	R-MCA	No	1	R-putamen
8	F/40	L-cortical segment	No	1	Multifocal
9	F/55	R-internal cerebral veins	No	1	Multifocal
10	F/66	No	R-cerebral peduncle	1	R-parietal lobe
11	M/53	No	L-internal capsule	1	L-thalamus
12	M/42	L-MCA	No	1	L-putamen
13	F/57	L- PCA	L-cerebral peduncle	2	L-thalamus
14	F/43	No	R-basal ganglia	1	R-putamen
15	F/41	L-MCA	L-external capsule	2	L-putamen
16	F/41	No	L-internal capsule	1	L-putamen
17	F/67	No	R-external capsule	1	R-putamen
18	F/29	No	L-external capsule	1	L-putamen
19	F/64	L-MCA	L-thalamus	2	L-putamen
20	M/48	L-MCA	No	1	L-putamen

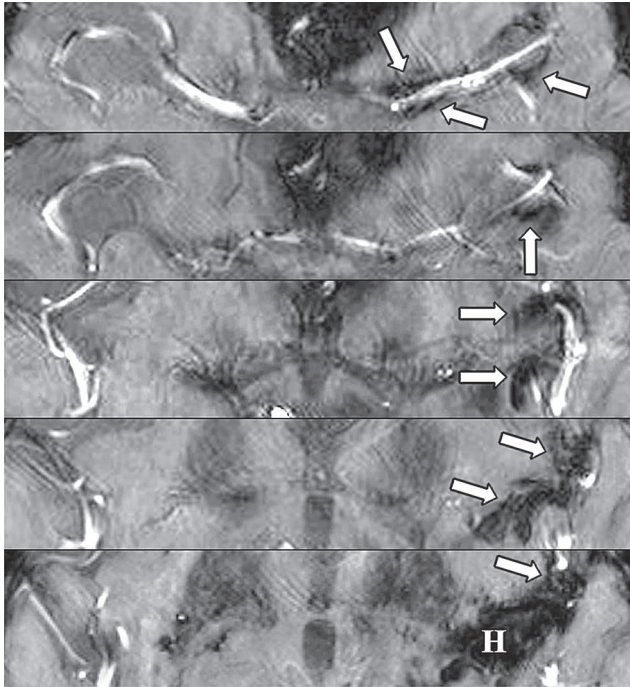


Fig. 1. Perivascular extension of hematoma around MCA. Serial SWIs of Patient 1 reveal the presence of a paramagnetic substance (white arrows) that is eliminated from the bottom of the hematoma (H) and surrounds the M2 and M1 segments of the left MCA. By contrast, no paramagnetic substance surrounds the contralateral MCA and its segments.

the 20 patients (Table 1).

Perivascular extension of hematoma

Remote hemorrhagic lesions were found around the middle cerebral artery (MCA). From the SWI results of Patient 1, we found that the paramagnetic substances from the hematoma occupied the sylvian cistern around the M2 segment of the left MCA and extended to the surroundings of the M1 segment of the left MCA. This result suggested that paramagnetic substances were distributed via VRS around the entire stretch of the MCA from the bottom of the hematoma (Fig. 1). The CT scan revealed a 9-ml hematoma in the left putamen of Patient 1. The SWI results of Patient 2 also revealed this phenomenon. Patient 2 had a 7-ml hematoma in the left putamen, displayed as a signal loss on the SWI images (Fig. 2a, H). We found two CMBs near the hematoma and observed a significant relationship between the location of these two lesions and the hematoma. We found that a paramagnetic substance in one lesion that was linked closely to the hematoma surrounded an arteriole passed through the hematoma (Fig. 2a, straight arrow). The arteriole, exhibited hyperintensity in the images, should be a branch of the M2 segment of the left MCA in the left sylvian cistern. The blood in the hematoma could possibly spread along the arteries. Another lesion in the left sylvian cistern, which is not a form of veins, was possibly formed by the leakage of the original hematoma from the rear end (Fig. 2a, curved arrow).

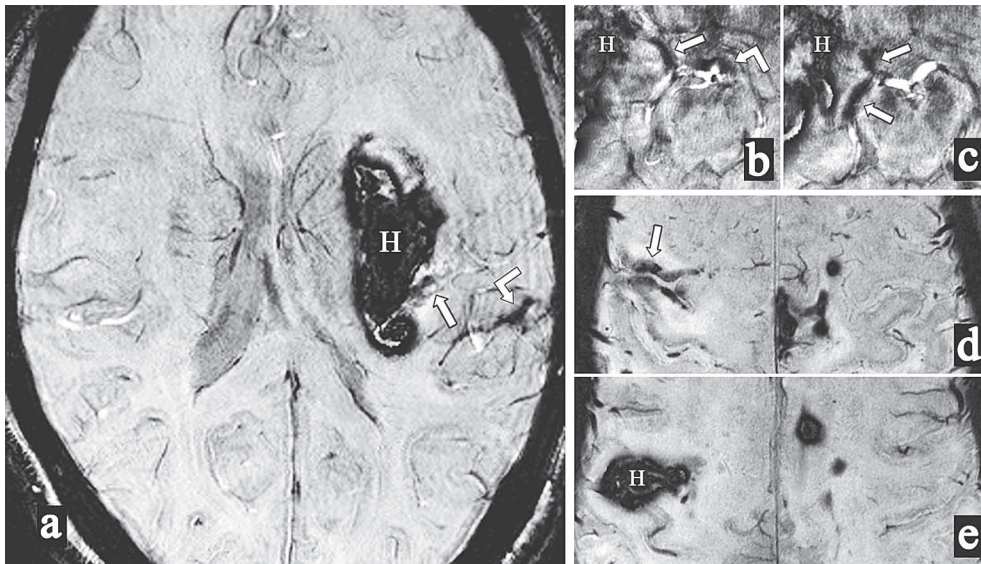


Fig. 2. Perivascular extension of hematoma around segments of cerebral arteries.

The hematoma of Patient 2 in the left putamen shown as hypointensity (a, H) for the hemoglobin and has almost completely deoxygenated (a). An artery that is perforated through the rear end of the hematoma is encysted by a paramagnetic substance originating from the hematoma (a, straight arrow). A paramagnetic substance accumulated in the sylvian cistern (a, curved arrow), which does not take the form of veins but exhibit perivascular extension from the rear end of the hematoma. No paramagnetic substance was observed in the contralateral sylvian cistern. Serial SWIs of Patient 3: the paramagnetic substance in the hematoma (b, c, H) leaks into the peripheral area of the right PCA (b, c, straight arrows) and the basilar artery (b, curved arrow). Serial SWIs of Patient 4: the paramagnetic substance around a cortex segment of the right MCA (d, straight arrows) originate from larger hemorrhagic lesions that are close to the surface of the cerebral cortex (e, H).

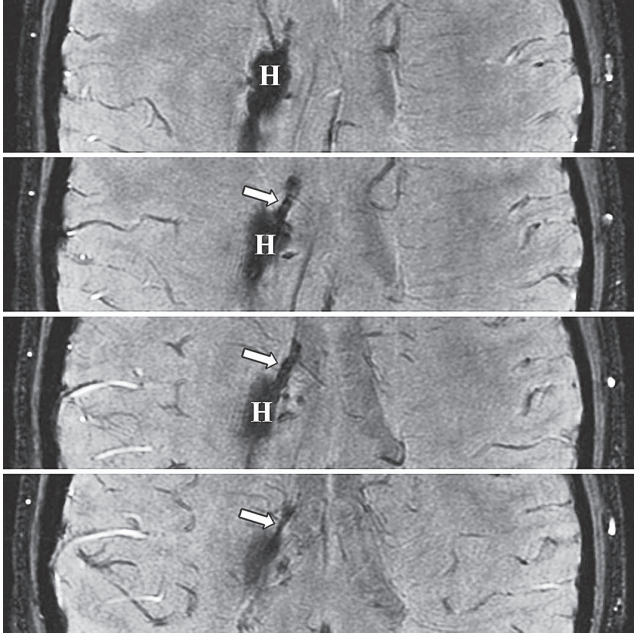


Fig. 3. Perivascular extension of hematoma around veins. Serial SWI images of Patient 5 indicated perivascular extension of hematoma around a venule (straight arrows)

The SWI results of Patient 3 revealed a distribution of remote hemorrhagic lesions along the right posterior cerebral artery (PCA) (Fig. 2b and c). The CT images showed a 9-ml hematoma in the right putamen of this patient.

Remote hemorrhagic lesions were also found around the cortex segments of the cerebral arteries (Fig. 2d and e). This finding was revealed by the SWI images of Patient 4, who had multifocal hemorrhagic lesions in the right frontal and left occipital lobes, bilateral basal ganglia, and centrum ovale majus.

Remote hemorrhagic lesions around veins were also revealed. From the SWI images of Patient 5, we found that the paramagnetic substance in the hematoma leaked into the right lateral ventricle along a branch of the right thalamostriate veins (Fig. 3, arrows). The CT images indicated a 12-ml hematoma in the right parietal lobe of this patient.

Perineural extension of hematoma

The SWI images of Patient 6, who had a 12-ml right putamen hematoma, revealed a remote hemorrhagic lesion in the ipsilateral tractus spinothalamicus in the right mid-brain (Fig. 4). The paramagnetic substance originated from the hematoma via the spaces around the ipsilateral sensory tracts passing through the right thalamus.

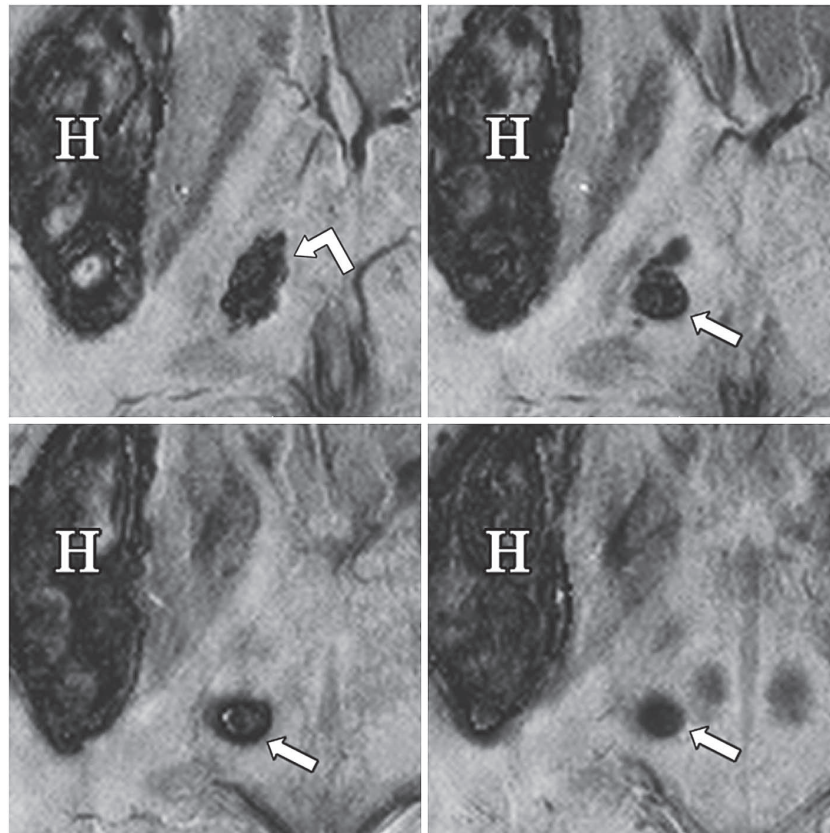


Fig. 4. Multiple hematomas in the right putamen and thalamus. Serial SWIs of Patient 6 reveal a primary hematoma in the right putamen (H, straight arrow). The paramagnetic substance of a secondary hematoma (curved arrow) in the right thalamus extended to the ipsilateral area of tractus spinothalamicus (straight arrows).

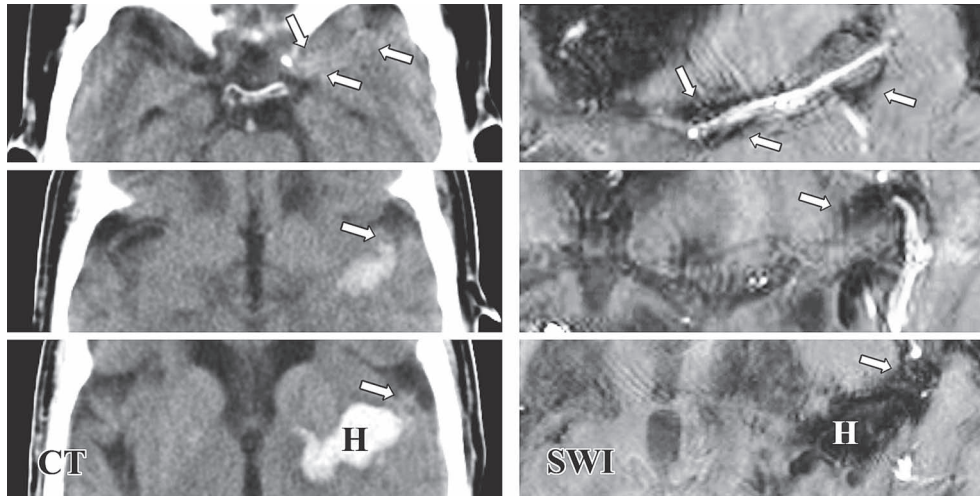


Fig. 5. CT scan cannot detect perivascular extension of hematoma.

Unenhanced CT scan (left) of Patient 1 with a hematoma in the left putamen detected no hematoma around the left MCA (straight arrows), whereas hypointense MRI signals were detected on the corresponding slices by using SWI (right).

CT scans revealed no hyperdensity around the blood vessels and perineurium

The non-enhanced CT scans of the 20 patients did not reveal any hyperdensity around the blood vessels and white matter (Fig. 5) outside the hematoma. This result was probably caused by the partial volume effect.

Discussion

In the present study, we successfully provide evidence for the perivascular and perineural extensions of hematomas in ICH patients. The results indicated that paramagnetic substances could spread from the original hematoma, thus forming remote hemorrhagic lesions along cerebral arteries and veins (Figs. 1, 2, and 3). Blood from the original hematoma could also expand to form remote hemorrhagic lesions in spaces around nerve tracts during hematoma invasion (Fig. 4).

Differences in tissue susceptibility were used in SWI to provide excellent contrasts between tissues with susceptibilities (Haacke et al. 2004). Hemoglobin molecules change into deoxyhemoglobin when blood leaks out of vessels, thus producing local non-uniform magnetic fields. Deoxyhemoglobin causes signal loss in T2-WI and gradient echo (GRE) T2*-WI. SWI allows the improved detection of paramagnetic hemorrhagic blood products, extravascular deoxyhemoglobin, and methemoglobin. SWI has emerged as an excellent modality for the detection of either acute or chronic ICH, as well as CMBs detected by MRI as focal areas of signal loss in brain parenchyma measuring <5 mm (Greer et al. 2004; Fiehler 2006; Park et al. 2009). CMBs were found in 47% to 80% of ICH patients and were regarded as markers of bleeding-prone microangiopathy such as lipohyalinosis and amyloid angiopathy (Offenbacher et al. 1996; Good et al. 1998; Greenberg et al. 1999; Koennecke 2006). However, these studies could not

provide evidence that blood in CMBs leak from small vessels instead of the original hematoma; thus, the mechanism of the formation of CMBs in ICH remains uncertain. Most lesions formed by the perivascular and perineural extensions of hematomas, measuring < 5 mm, belong in CMBs. With the excellent modality for the detection of CMBs with SWI, the result of this study indicates that the leakage of hematoma in the VRS and perineurium can result in the formation of CMBs, providing a new explanation for the mechanism of the CMBs in patients with ICH.

A ring hemorrhage is remote hemorrhagic lesion in ICH that is observed extensively in peripheral tissues around hematomas (Treip 1978; Copenhagen et al. 2008; Imaizumi et al. 2008; Smith et al. 2010). Some ring hemorrhages have aspects of CMBs on MRI images. Our previous study with a rat model of ICH showed that the lesions of ring hemorrhages were formed by perivascular and perineural extensions of hematomas via the VRS or perineurium (He et al. 2012). Blood elements were drained into the lymph sinuses in the bilateral deep cervical lymph nodes. Lymphostasis was also observed in the brain tissues around the hematoma and peaked 3 days after ICH.

Various anatomic clearances exist in brain tissues such as VRS and spaces around nerve tracts. VRS, also called perivascular spaces, surround the walls of arteries, arterioles, veins, and venules stretching from the subarachnoid space into the brain parenchyma (Virchow 1851; Robin 1859; Zhang et al. 1990; Kwee and Kwee 2007; He et al. 2012). VRS are the main pathways for the elimination of interstitial fluid and solutes such as amyloid-beta (A β) from the grey matter of the brain (Schley et al. 2006; Weller et al. 2009). Blood in hematomas may leak out via VRS (He et al. 2012), thus forming the perivascular extension of hematomas.

Spaces around nerve tracts in cerebral parenchyma

formed by loose connective tissues are types of extracellular spaces (ECS). Molecular diffusion in ECS is important for non-synaptic intercellular communication, extracellular ionic buffering, and drug and metabolite delivery (Lehmenkühler et al. 1993). Blood could also easily overflow in ECS, thus forming the perineural extension of hematomas.

The perivascular and perineural extensions of hematomas can provide the mechanism of the series of pathological processes involved in ICH. Firstly, the perivascular and perineural extensions of hematomas could explain the remote effects of ICH. Extensive brain edema and brain damage could occur in either the perihematomal or remote brain regions after ICH, thus leading to neurological deficits (Qureshi et al. 2001; Wagner et al. 2003; Mun-Bryce et al. 2004; Hua et al. 2006; Xi et al. 2006). Toxic hematoma extravasations, such as iron (Wagner et al. 2003; Nakamura et al. 2005; Hua et al. 2006; Okauchi et al. 2009), inflammatory cytokines, and thrombin (Mun-Bryce et al. 2004; Xi et al. 2006; Zhang et al. 2006), contribute to the occurrence of neurological deficits. Nevertheless, the mechanism of how toxic hematoma extravasations cause the remote effects of ICH is still unknown. The perivascular and perineural extensions of hematomas may provide a new explanation for the mechanism of toxic hematoma extravasations. The coverage area of toxic hematoma extravasations, which are hard to diffuse in brain parenchyma, can be remarkably expanded during the perivascular and perineural extensions of hematomas. When ICH occurs, blood leaks from cerebral arteries into VRS, inducing damaging effects on the whole brain. Secondly, the perivascular and perineural extensions of hematomas provided new explanations for the formation of CMBs in ICH besides the hypothesis of microangiopathy. The results of this study provided evidence on the relationship between CMBs and the original hematoma; this relationship is formed by the leakage of original hematomas via the VRS or perineurium.

In summary, the present study has shown that blood from hematomas can leak via the VRS or perineurium, thus resulting in the formation of CMBs. Our results provided a new explanation for the detection of CMBs in patients with ICH. Obtaining detailed information on the distribution and characteristics of the perivascular and perineural extensions of hematomas by radiological techniques is difficult. Joint research including pathologic examination and radiological techniques may provide more comprehensive and reliable evidence to confirm our findings.

Acknowledgements

This study was funded by the National Natural Science Foundation of China (Grant No. 61072033) and the Natural Science Foundation of Guangdong Province, P.R. China (Grant Nos. 8151051501000053 and 10151051501000076).

Conflict of Interest

The authors declare that they have no financial or conflict of interest.

References

- Copenhaver, B.R., Hsia, A.W., Merino, J.G., Burgess, R.E., Fifi, J.T., Davis, L., Warach, S. & Kidwell, C.S. (2008) Racial differences in microbleed prevalence in primary intracerebral hemorrhage. *Neurology*, **71**, 1176-1182.
- Fiehler, J. (2006) Cerebral microbleeds: old leaks and new haemorrhages. *Int. J. Stroke*, **1**, 122-130.
- Good, C.D., Ng, V.W., Clifton, A., Britton, J.A., Hart, Y. & Wilkins, P. (1998) Amyloid angiopathy causing widespread miliary haemorrhages within the brain evident on MRI. *Neuroradiology*, **40**, 308-311.
- Greenberg, S.M., O'Donnell, H.C., Schaefer, P.W. & Kraft, E. (1999) MRI detection of new hemorrhages: potential marker of progression in cerebral amyloid angiopathy. *Neurology*, **53**, 1135-1138.
- Greer, D.M., Koroshetz, W.J., Cullen, S., Gonzalez, R.G. & Lev, M.H. (2004) Magnetic resonance imaging improves detection of intracerebral hemorrhage over computed tomography after intra-arterial thrombolysis. *Stroke*, **35**, 491-495.
- Haacke, E.M., Xu, Y., Cheng, Y.C. & Reichenbach, J.R. (2004) Susceptibility Weighted Imaging (SWI). *Magn. Reson. Med.*, **52**, 612-618.
- He, G., Lü, T., Lu, B., Xiao, D., Yin, J., Liu, X., Qiu, G., Fang, M. & Wang, Y. (2012) Perivascular and perineural extension of formed and soluble blood elements in an intracerebral hemorrhage rat model. *Brain Res.*, **1451**, 10-18.
- Hua, Y., Nakamura, T., Keep, R.F., Wu, J., Schallert, T., Hoff, J.T. & Xi, G. (2006) Long-term effects of experimental intracerebral hemorrhage: The role of iron. *J. Neurosurg.*, **104**, 305-312.
- Imaizumi, T., Honma, T., Horita, Y., Kawamura, M., Kohama, I., Miyata, K., Nyon, K.S. & Niwa, J. (2008) The number of microbleeds on gradient T2*-weighted magnetic resonance image at the onset of intracerebral hemorrhage. *J. Stroke Cerebrovasc. Dis.*, **17**, 30-34.
- Koennecke, H.C. (2006) Cerebral microbleeds on MRI: prevalence, associations, and potential clinical implications. *Neurology*, **66**, 165-171.
- Kwee, R.M. & Kwee, T.C. (2007) Virchow-Robin Spaces at MR Imaging. *Radiographics*, **27**, 1071-1086.
- Lehmenkühler, A., Syková, E., Svoboda, J., Zilles, K. & Nicholson, C. (1993) Extracellular space parameters in the rat neocortex and subcortical white matter during postnatal development determined by diffusion analysis. *Neuroscience*, **55**, 339-351.
- Lü, T.M., Lu, B.X. & Li, Z.Q. (2005) Pathogenesis of ring hemorrhage in perihematomal tissue after intracerebral hemorrhage. *Chin. J. Geriatr. Heart Brain Vessel Dis.*, **7**, 417-418.
- Lü, T.M., Lu, B.X. & Yin, J. (2007) Piping phenomenon in process of hematoma formation of intracerebral hemorrhage. *Chin. J. Geriatr. Heart Brain Vessel Dis.*, **9**, 489-491.
- Menon, R.S., Burgess, R.E., Wing, J.J., Gibbons, M.C., Shara, N.M., Fernandez, S., Jayam-Trouth, A., German, L., Sobotka, I., Edwards, D. & Kidwell, C.S. (2012) Predictors of highly prevalent brain ischemia in intracerebral hemorrhage. *Ann. Neurol.*, **71**, 199-205.
- Mun-Bryce, S., Wilkerson, A., Pacheco, B., Zhang, T., Rai, S., Wang, Y. & Okada, Y. (2004) Depressed cortical excitability and elevated matrix metalloproteinases in remote brain regions following intracerebral hemorrhage. *Brain Res.*, **1026**, 227-234.
- Nakamura, T., Keep, R.F., Hua, Y., Hoff, J.T. & Xi, G. (2005) Oxidative DNA injury after experimental intracerebral hemor-

- rhage. *Brain Res.*, **1039**, 30-36.
- Offenbacher, H., Fazekas, F., Schmidt, R., Koch, M., Fazekas, G. & Kapeller, P. (1996) MR of cerebral abnormalities concomitant with primary intracerebral hematomas. *Am. J. Neurodiol.*, **17**, 573-578.
- Okauchi, M., Hua, Y., Keep, R.F., Morgenstern, L.B. & Xi, G. (2009) Effects of deferoxamine on intracerebral hemorrhage-induced brain injury in aged rats. *Stroke*, **40**, 1858-1863.
- Park, J.H., Park, S.W., Kang, S.H., Nam, T.K., Min, B.K. & Hwang, S.N. (2009) Detection of traumatic cerebral microbleeds by susceptibility-weighted image of MRI. *J. Korean Neurosurg. Soc.*, **46**, 365-369.
- Qureshi, A.I., Tuhrim, S., Broderick, J.P., Batjer, H., Hondo, H. & Hanley, D.F. (2001) Spontaneous intracerebral hemorrhage. *N. Eng. J. Med.*, **344**, 1450-1460.
- Robin, C. (1859) Recherches sur quelques particularités de la structure des capillaires de l'encephale. *J. Physiol. Homme. Anim.*, **2**, 537-548.
- Schley, D., Carare-Nnadi, R., Please, C.P., Perry, V.H. & Weller, R.O. (2006) Mechanisms to explain the reverse perivascular transport of solutes out of the brain. *J. Theor. Biol.*, **238**, 962-974.
- Smith, E.E., Nandigam, K.R., Chen, Y.W., Jeng, J., Salat, D., Halpin, A., Frosch, M., Wendell, L., Fazen, L., Rosand, J., Viswanathan, A. & Greenberg, S.M. (2010) MRI markers of small vessel disease in lobar and deep hemispheric intracerebral hemorrhage. *Stroke*, **41**, 1933-1938.
- Treip, C.S. (1978) *Neuropathology*, Wolfe Medical Publications Ltd, Holland.
- Virchow, R. (1851) Ueber die Erweiterung kleinerer Gefaesse. *Archiv Pathol. Anat. Physiol. Klin. Med.*, **3**, 427-462.
- Wagner, K.R., Sharp, F.R., Ardizzzone, T.D., Lu, A. & Clark, J.F. (2003) Heme and iron metabolism: Role in cerebral hemorrhage. *J. Cereb. Blood Flow Metab.*, **23**, 629-652.
- Weller, R.O., Djuanda, E., Yow, H.Y. & Carare, R.O. (2009) Lymphatic drainage of the brain and the pathophysiology of neurological disease. *Acta Neuropathol.*, **117**, 1-14.
- Xi, G., Keep, R.F. & Hoff, J.T. (2006) Mechanisms of brain injury after intracerebral hemorrhage. *Lancet Neurol.*, **5**, 53-63.
- Zhang, E.T., Inman, C.B. & Weller, R.O. (1990) Interrelationship of the pia mater and the perivascular (Virchow-Robin) spaces in the human cerebrum. *J. Anat.*, **170**, 111-123.
- Zhang, X., Li, H., Hu, S., Zhang, L., Liu, C., Zhu, C., Liu, R. & Li, C. (2006) Brain edema after intracerebral hemorrhage in rats: the role of inflammation. *Neurol. India*, **54**, 402-407.
-